

Consistent forcing scheme in the cascaded lattice Boltzmann method

Linlin Fei¹ and Kai Hong Luo^{1,2,*}

¹*Center for Combustion Energy, Key laboratory for Thermal Science and Power Engineering of Ministry of Education, Department of Thermal Engineering, Tsinghua University, Beijing 100084, China*

²*Department of Mechanical Engineering, University College London, Torrington Place, London WC1E 7JE, UK*

(Received 31 May 2017; published 13 November 2017)

In this paper, we give an alternative derivation for the cascaded lattice Boltzmann method (CLBM) within a general multiple-relaxation-time (MRT) framework by introducing a shift matrix. When the shift matrix is a unit matrix, the CLBM degrades into an MRT LBM. Based on this, a consistent forcing scheme is developed for the CLBM. The consistency of the nonslip rule, the second-order convergence rate in space, and the property of isotropy for the consistent forcing scheme is demonstrated through numerical simulations of several canonical problems. Several existing forcing schemes previously used in the CLBM are also examined. The study clarifies the relation between MRT LBM and CLBM under a general framework.

DOI: [10.1103/PhysRevE.96.053307](https://doi.org/10.1103/PhysRevE.96.053307)

I. INTRODUCTION

The lattice Boltzmann method (LBM), based on the simplified kinetic models, has gained remarkable success for numerical simulations of complex fluid flows and beyond, with applications to (but not limited to) microflows, flows in porous media, turbulence, multiphase flows, and reactive flows [1–9]. The LBM solves a specific discrete Boltzmann equation for distribution functions, designed to recover the Navier-Stokes (N-S) equations in the macroscopic limit. The mesoscale nature of LBM allows its natural incorporation of micro and mesoscale physics, while the highly efficient algorithm makes it affordable computationally [9].

In the standard “collision-streaming” LBM algorithm, the simplest collision operator is the Bhatnagar-Gross-Krook (BGK) or single-relaxation-time (SRT) operator, in which all the distribution functions relax at an identical rate to their local equilibrium counterparts and the relaxation rate is related to the kinematic viscosity [10]. The multiple-relaxation-time (MRT) operator is another extensively used operator [11], in which the collision is executed in the raw moment space and the relaxation rates for different moments can be different. More recently, a central-moment-based or cascaded operator was proposed by Geier *et al.* [12]. In the cascaded lattice Boltzmann method (CLBM), the collision is carried out in the space of central moment rather than that of raw moment as in the MRT LBM. Compared with the BGK operator, the MRT and cascaded operators can enhance the numerical stability significantly [12–15]. Although the collision steps in these LBMs are quite different, the streaming steps are carried out in the same way by streaming the post-collision distributions to their neighbors. It should be noted that other collision operators, such as the two-relaxation-time (TRT) operator [16,17] and the entropic operator [18,19], are also very popular in the lattice Boltzmann community.

In many fluid systems, an external or internal force field plays an important role in the flow behaviors. To incorporate the forcing effect, different forcing treatments or forcing schemes have been proposed in the previous literatures

[4,20–24]. In 2002, Guo *et al.* analyzed the discrete lattice effects on the forcing scheme and developed a representation of the forcing term [25]. Guo *et al.* then extended the method to the MRT LBM in 2008 [26]. For the CLBM, there is still no commonly used forcing scheme, while one scheme by method of central moments has been proposed by Premnath *et al.* [27]. In Ref. [28], Lycett-Brown and Luo adopted the forcing scheme for the BGK LBM in the CLBM directly. As analyzed by De Rosis [29], the method proposed by Premnath *et al.* may encounter cumbersome practical implementations. Based on the central moments of a discrete equilibrium, a forcing scheme has been developed in Ref. [29].

However, there is still no analysis about whether these forcing schemes in the CLBM are consistent with the extensively used forcing schemes in the MRT LBM [26] and BGK LBM [25]. In this paper, we propose an alternative derivation for the CLBM by introducing a shift matrix. This approach clarifies the relationship between the MRT LBM and CLBM. Based on this framework, we present a consistent forcing scheme in CLBM and show that the previous methods in Refs. [27–29] are not consistent. The rest of the paper is structured as follows. Section II gives the new derivation for the CLBM and presents the consistent forcing scheme. Section III presents theoretical analyses for the previous forcing schemes. Numerical verifications are presented in Sec. IV. Finally, conclusions are made in Sec. V.

II. CLBM AND CONSISTENT FORCING SCHEME

A. Cascaded LBM

Without losing generality, the D2Q9 lattice [10] is adopted here. The lattice speed $c = \Delta x / \Delta t = 1$ and the lattice sound speed $c_s = 1/\sqrt{3}$ are adopted, where Δx and Δt are the lattice space and time steps. The discrete velocities $\mathbf{e}_i = [|e_{ix}\rangle, |e_{iy}\rangle]$ are defined as

$$\begin{aligned} |e_{ix}\rangle &= [0, 1, 0, -1, 0, 1, -1, -1, 1]^\top, \\ |e_{iy}\rangle &= [0, 0, 1, 0, -1, 1, 1, -1, -1]^\top, \end{aligned} \quad (1)$$

where $i = 0 \dots 8$, $|\cdot\rangle$ denotes a nine-dimensional column vector, and the superscript \top denotes the transposition.

Here we propose a new derivation for the CLBM, which is different from and more intelligible than that given by Geier

*k.luo@ucl.ac.uk

et al. [12]. We first define the raw and central velocity moments of the discrete distribution functions (DFs) f_i ,

$$k_{mn} = \langle f_i | e_{ix}^m e_{iy}^n \rangle, \quad \tilde{k}_{mn} = \langle f_i | (e_{ix} - u_x)^m (e_{iy} - u_y)^n \rangle, \quad (2)$$

where u_x and u_y are the horizontal and vertical velocity components. The equilibrium counterparts k^{eq} and \tilde{k}_{mn}^{eq} are defined analogously by replacing f_i with the discrete equilibrium distribution functions (EDFs) f_i^{eq} in Eq. (2). In the previous CLBM, the recombined raw moments are adopted,

$$|T_i\rangle = [k_{00}, k_{10}, k_{01}, k_{20} + k_{02}, k_{20} - k_{02}, k_{11}, k_{21}, k_{12}, k_{22}]^T, \quad (3)$$

so do the recombined central moments \tilde{T}_i . The transformation from the discrete DFs to their raw moments can be performed through a transformation matrix \mathbf{M} , and the shift from the raw moments to central moments can be performed through a shift matrix \mathbf{N} ,

$$|T_i\rangle = \mathbf{M}|f_i\rangle, \quad |\tilde{T}_i\rangle = \mathbf{N}|T_i\rangle. \quad (4)$$

$$\mathbf{N} = \begin{bmatrix} 1 & 0 & 0 & 0 & 0 & 0 & 0 & 0 & 0 \\ -u_x & 1 & 0 & 0 & 0 & 0 & 0 & 0 & 0 \\ -u_y & 0 & 1 & 0 & 0 & 0 & 0 & 0 & 0 \\ u_x^2 + u_y^2 & -2u_x & -2u_y & 1 & 0 & 0 & 0 & 0 & 0 \\ u_x^2 - u_y^2 & -2u_x & 2u_y & 0 & 1 & 0 & 0 & 0 & 0 \\ u_x u_y & -u_y & -u_x & 0 & 0 & 1 & 0 & 0 & 0 \\ -u_x^2 u_y & 2u_x u_y & u_x^2 & -u_y/2 & -u_y/2 & -2u_x & 1 & 0 & 0 \\ -u_y^2 u_x & u_y^2 & 2u_x u_y & -u_x/2 & u_x/2 & -2u_y & 0 & 1 & 0 \\ u_x^2 u_y^2 & -2u_x u_y^2 & -2u_y u_x^2 & u_x^2/2 + u_y^2/2 & u_y^2/2 - u_x^2/2 & 4u_x u_y & -2u_y & -2u_x & 1 \end{bmatrix}. \quad (6)$$

In the collision step for CLBM, the central moments \tilde{T}_i are relaxed to their equilibrium values \tilde{T}_i^{eq} . Thus, the post-collision central moments are

$$\begin{aligned} |\tilde{T}_i^*\rangle &= (\mathbf{I} - \mathbf{S})|\tilde{T}_i\rangle + \mathbf{S}|\tilde{T}_i^{eq}\rangle \\ &= (\mathbf{I} - \mathbf{S})\mathbf{N}\mathbf{M}|f_i\rangle + \mathbf{S}\mathbf{N}\mathbf{M}|f_i^{eq}\rangle, \end{aligned} \quad (7)$$

where $\mathbf{S} = \text{diag}(s_0, s_1, s_1, s_b, s_2, s_2, s_3, s_3, s_4)$ is a diagonal relaxation matrix. The kinematic and bulk viscosities are related to the relaxation parameters $s_2 = 1/(3\nu + 0.5)$ and $s_b = 1/(3\xi + 0.5)$, respectively. As recommended in Refs. [12,27,28], the central moments of f_i^{eq} are set equal to the continuous central moments of the Maxwell-Boltzmann distribution in continuous velocity space. To be specific,

$$|\tilde{T}_i^{eq}\rangle = [\rho, 0, 0, 2\rho c_s^2, 0, 0, 0, 0, \rho c_s^4]^T, \quad (8)$$

where ρ is the fluid density, thus the matrix manipulation is not needed for f_i^{eq} . The corresponding discrete EDF is in fact a generalized local equilibrium [27,30]. Due to the definitions of the transformation and shift matrices, both of them are invertible (explicit expressions for \mathbf{M}^{-1} and \mathbf{N}^{-1} are given in the Appendix). The post-collision discrete DFs are given by

$$|f_i^*\rangle = \mathbf{M}^{-1}\mathbf{N}^{-1}|\tilde{T}_i^*\rangle. \quad (9)$$

The formulations for \mathbf{M} and \mathbf{N} depend on the considered raw-moment set in Eq. (3), which are not unique. In the present study, the transformation matrix \mathbf{M} is expressed as [28]

$$\mathbf{M} = \begin{bmatrix} 1 & 1 & 1 & 1 & 1 & 1 & 1 & 1 & 1 \\ 0 & 1 & 0 & -1 & 0 & 1 & -1 & -1 & 1 \\ 0 & 0 & 1 & 0 & -1 & 1 & 1 & -1 & -1 \\ 0 & 1 & 1 & 1 & 1 & 2 & 2 & 2 & 2 \\ 0 & 1 & -1 & 1 & -1 & 0 & 0 & 0 & 0 \\ 0 & 0 & 0 & 0 & 0 & 1 & -1 & 1 & -1 \\ 0 & 0 & 0 & 0 & 0 & 1 & 1 & -1 & -1 \\ 0 & 0 & 0 & 0 & 0 & 1 & -1 & -1 & 1 \\ 0 & 0 & 0 & 0 & 0 & 1 & 1 & 1 & 1 \end{bmatrix}. \quad (5)$$

Asinari proposed a ‘‘shift matrix,’’ where the focus was on the relation between the cascaded operator and TRT operator [30]. Another raw-moment set $|T_i\rangle = [k_{00}, k_{10}, k_{01}, k_{20}, k_{02}, k_{11}, k_{21}, k_{12}, k_{22}]^T$ was adopted in Ref. [30], leading to a different formulation for the ‘‘shift matrix’’ in Ref. [30]. In this paper, the formulation for \mathbf{N} is

In the streaming step, the post-collision discrete DFs in space \mathbf{x} stream to the neighbor nodes ($\mathbf{x} + \mathbf{e}_i \Delta t$) along the discrete velocity direction as usual [25,26,31],

$$f_i(\mathbf{x} + \mathbf{e}_i \Delta t, t + \Delta t) = f_i^*(\mathbf{x}, t). \quad (10)$$

Using the Chapman-Enskog analysis, the incompressible N-S equations can be reproduced in the low-Mach number limit [27,28]. The hydrodynamics variables are obtained as

$$\rho = \sum_i f_i, \quad \rho \mathbf{u} = \sum_i f_i \mathbf{e}_i. \quad (11)$$

It can be readily shown that when the shift matrix \mathbf{N} is a unit matrix, the CLBM degrades into a nonorthogonal MRT LBM as in Refs. [28,31]. Thus, within a general multiple-relaxation-time framework, the present derivation clarifies the relationship between the MRT LBM and CLBM.

B. Consistent forcing scheme

Inspired by the method proposed by He *et al.* [23,24], to incorporate an external or internal force field $\mathbf{F} = [F_x, F_y]$ into the CLBM with a high-order accuracy, a second-order trapezoidal scheme is adopted. Thus, the evolution equation

for central moments can be given as

$$|\tilde{T}_i(\mathbf{x} + \mathbf{e}_i \Delta t, t + \Delta t)\rangle = (\mathbf{I} - \mathbf{S})|\tilde{T}_i(\mathbf{x}, t)\rangle + \mathbf{S}|\tilde{T}_i^{\text{eq}}(\mathbf{x}, t)\rangle + \Delta t/2[C_i(\mathbf{x}, t) + C_i(\mathbf{x} + \mathbf{e}_i \Delta t, t + \Delta t)], \quad (12)$$

where C_i are central moments of the forcing terms R_i . According to the assumption by He *et al.* [23,24], R_i can be given by

$$R_i = \frac{\mathbf{F}(\mathbf{e}_i - \mathbf{u})}{\rho c_s^2} f_i^{\text{eq}}. \quad (13)$$

When using the generalized local equilibrium, C_i can be obtained explicitly as

$$|C_i\rangle = \mathbf{N}\mathbf{M}|R_i\rangle = [0, F_x, F_y, 0, 0, 0, c_s^2 F_y, c_s^2 F_x, 0]^\top. \quad (14)$$

In the practical implementation, the following transformation method is adopted to remove the implicitness in Eq. (12),

$$\bar{f}_i = f_i - 1/2 R_i, \quad \bar{T}_i = \tilde{T}_i - 1/2 C_i. \quad (15)$$

By substituting Eq. (15) into Eq. (12), the collision step in central moments is modified by

$$|\bar{T}_i^*\rangle = (\mathbf{I} - \mathbf{S})\mathbf{N}\mathbf{M}|\bar{f}_i\rangle + \mathbf{S}\mathbf{N}\mathbf{M}|f_i^{\text{eq}}\rangle + (\mathbf{I} - \mathbf{S}/2)\mathbf{N}\mathbf{M}|R_i\rangle = (\mathbf{I} - \mathbf{S})|\bar{T}_i\rangle + \mathbf{S}|\tilde{T}_i^{\text{eq}}\rangle + (\mathbf{I} - \mathbf{S}/2)|C_i\rangle. \quad (16)$$

By using $|\bar{f}_i^*\rangle = \mathbf{M}^{-1}\mathbf{N}^{-1}|\bar{T}_i^*\rangle$, the streaming step can be executed as usual,

$$\bar{f}_i(\mathbf{x} + \mathbf{e}_i \Delta t, t + \Delta t) = \bar{f}_i^*(\mathbf{x}, t). \quad (17)$$

Then the fluid velocity is redefined by

$$\rho \mathbf{u} = \sum_i \bar{f}_i \mathbf{e}_i + \Delta t \mathbf{F}/2. \quad (18)$$

Remark 1. In Eq. (12), the forcing terms in the present scheme are considered by means of central moments, which is compatible with the basic ideology (collision in the central-moment space) in the CLBM.

Remark 2. When the shift matrix \mathbf{N} in Eq. (16) is a unit matrix, the CLBM with the present forcing scheme will degrade into the MRT LBM proposed by Liu *et al.* [31] with some high-order terms. It is known that the method of Liu *et al.* [31] is equivalent to the method of Guo *et al.* in Ref. [26].

Remark 3. In the original forcing scheme proposed by Guo *et al.* [25], the forcing terms are defined as $R_{Gi} = w_i[(\mathbf{e}_i - \mathbf{u})/c_s^2 + (\mathbf{e}_i \cdot \mathbf{u})\mathbf{e}_i/c_s^4]\mathbf{F}$. It is easy to find that the forcing terms in Eq. (13) are equivalent to R_{Gi} plus some high-order terms. The constraint conditions for the forcing terms (see Eq. (7) in Ref. [25]) are also satisfied in the present scheme. In particular, if all the parameters in the matrix \mathbf{S} are set equal to s_2 , the CLBM with the present forcing scheme degrades into the BGK LBM with a generalized local equilibrium and the forcing scheme by Guo *et al.*

Remark 4. It is also found (see Sec. IV) that the zero-slip velocity boundary condition for the half-way bounce-back rule [$s_3 = (16 - 8s_2)/(8 - s_2)$] discussed in Refs. [26,32] is also applicable to the present forcing scheme.

From the above reasons, we proclaim the present forcing scheme as a consistent scheme in the CLBM.

III. OTHER FORCING SCHEMES

In this section, several existing methods to incorporate forcing terms into the CLBM in the literature are summarized. To show the inconsistencies in these forcing schemes, they are all written in the general multiple-relaxation-time frame proposed in Sec. II.

A. Forcing scheme by Premnath *et al.*

In 2009, Premnath *et al.* [27] proposed a forcing scheme to incorporate forcing terms into CLBM. Inspired by He *et al.* [24], they proposed a change of continuous distribution function f due to the presence of a force field,

$$\Delta f = \frac{\mathbf{F}}{\rho} \cdot \frac{(\mathbf{e}_i - \mathbf{u})}{c_s^2} f^M, \quad (19)$$

where f^M is the Maxwell-Boltzmann distribution in continuous velocity space. The central moments of Δf , C_{Pi} , are then incorporated into the collision stage by

$$|\bar{T}_i^*\rangle = (\mathbf{I} - \mathbf{S})|\bar{T}_i\rangle + \mathbf{S}|\tilde{T}_i^{\text{eq}} - C_{Pi}/2\rangle. \quad (20)$$

The discrete counterparts for Δf , Δf_i are also needed (see Eq.(37) in Ref. [27]) to obtain the post-collision discrete DFs,

$$|\bar{f}_i^*\rangle = \mathbf{M}^{-1}\mathbf{N}^{-1}|\bar{T}_i^*\rangle + |\Delta f_i\rangle. \quad (21)$$

The fluid velocity is defined as in Eq. (18).

It should be noted that the original derivation in Ref. [27] is tedious, and C_{Pi} and Δf_i correspond to $\hat{\sigma}_{x^m y^n}$ and S_a in Ref. [27], respectively. Although the method is compatible with the central-moment-based collision operator, the explicit formulations of Δf_i and their raw moments are needed, which makes the practical implementations cumbersome [29]. Moreover, in their definition for C_{Pi} , the high-order nonzero terms are removed arbitrarily,

$$|C_{Pi}\rangle = \mathbf{N}\mathbf{M}|\Delta f_i\rangle = [0, F_x, F_y, 0, 0, 0, 0, 0, 0]^\top. \quad (22)$$

Although they think that the high-order terms do not affect consistency, we certainly see some inconsistencies. For example, the key elements in Δf_i and R_{Gi} are apparently inconsistent,

$$\begin{aligned} \Delta f_0 &= -2F_x u_x - 2F_y u_y + O(u^3), \\ R_{G0} &= -3F_x u_x - 3F_y u_y, \end{aligned} \quad (23)$$

which will affect numerical performances (see in Sec. IV).

B. Forcing scheme by Lycett-Brown and Luo

Cascaded LBM was first used to simulated multiphase flows by Lycett-Brown *et al.* [28]. In their method, three forcing schemes, the Shan-Chen method [4], the EDM method [33], and the Guo method [25], were adopted directly in the CLBM.

As discussed in the literature [34,35], both the Shan-Chen method and EDM method will lead to some additional terms in the recovered macroscopic equations. The additional terms may have some positive effects on the numerical performance of the Shan-Chen model [4], but it is not recommended to use the Shan-Chen method and EDM method in the CLBM directly for general flows. In the present work, we only consider the

CLBM with the forcing scheme of Guo *et al.* Thus, the collision stage in central moments can be written as

$$|\bar{T}_i^* \rangle = (\mathbf{I} - \mathbf{S})|\bar{T}_i \rangle + \mathbf{S}|\bar{T}_i^{\text{eq}} \rangle + (1 - s_2/2)\mathbf{NM}|R_{Gi} \rangle, \quad (24)$$

and the fluid velocity is also defined as in Eq. (18).

C. Forcing scheme by De Rosis

Recently, De Rosis proposed an alternative method to incorporate forcing terms into the CLBM. The collision stage in central moments is

$$|\bar{T}_i^* \rangle = (\mathbf{I} - \mathbf{S})|\bar{T}_i \rangle + \mathbf{S}|\bar{T}_i^{\text{eq}} \rangle + \frac{1}{2}|\xi_i \rangle, \quad (25)$$

where ξ_i are the central moments of the forcing terms, and the fluid velocity is also defined as in Eq. (18).

Unfortunately, there is a typographical error in Eq. (16) of the paper [29]. Particularly, the sign in front of $\xi_i/2$ is not correct. In this method, the forcing terms are defined by the truncated local equilibrium DF, which leads to a lot of velocity terms in ξ_i (see Eq. (15) in Ref. [29]). Due to the definition of central moments, it is not recommended to include velocity terms in ξ_i . Thus, there are some spurious effects using this method. It is also noted that the computational load for ξ_i is much higher than that of C_i in Eq. (14). Comparing Eq. (25) with Eq. (16), it is seen that the relaxation rate for each element of ξ_i is 1.0 in this method, which is not consistent with the multiple-relaxation-time methodology in the CLBM.

D. Discussions

Remark 5. In the CLBM, the first three central moments are conserved moments, corresponding to conservations of mass and momentum. Thus, the first two parameters (s_0 and s_1) in the relaxation matrix \mathbf{S} can be chosen freely. This property is retained in the present forcing scheme and the forcing scheme by Premnath *et al.* [27], because the relaxation matrix acts on the forcing terms in these two methods [see Eqs. (16) and (20)]. However, s_1 needs to be set equal to s_2 in the forcing scheme by Lycett-Brown and Luo [28] and to be 1.0 in the forcing scheme by De Rosis [29], to guarantee the conservation of momentum.

Remark 6. If s_3 is set to be 2.0, the forcing effect on the third-order central moments in Eq. (16) is removed. Thus, the present scheme degrades into the forcing scheme by Premnath *et al.* [27] only when $s_3 = 2.0$. Similarly, only when $s_3 = 1.0$, the difference between the forcing scheme by De Rosis [29] and the present scheme can be removed. Finally, only in the BGK limitation when all the parameters are equal to s_2 , the present scheme degrades into the scheme by Lycett-Brown and Luo [28]. In general, the deviations between the above three forcing schemes and the present consistent forcing scheme should be approximately proportional to $(s_3 - 2)/2$, $(s_3 - s_2)/2$ and $(s_3 - 1)/2$, respectively.

Remark 7. In 2015, an improved forcing scheme for the pseudopotential model [4] in multiphase flow was proposed by Lycett Brown and Luo [36]. The improved forcing scheme was then incorporated into the CLBM for multiphase flow with large-density-ratio at high Reynolds and Weber numbers [14]. The basic philosophy of the improved forcing scheme is introducing artificial terms in the pressure tensor to counteract

the lack of thermodynamical consistency in the original pseudopotential model. Thus, it is not suitable for general flows with a force field. Besides, another simple forcing method was used in the CLBM to simulate turbulent channel flow in 2011 [37]. However, as analyzed by Guo *et al.* [25], the method used in Ref. [37] cannot recover the accurate macroscopic equations with a spatial and/or temporal variational force field in the BGK LBM, not to mention in the CLBM.

IV. NUMERICAL SIMULATIONS

In this section, we conduct several benchmark cases to verify the consistent forcing scheme. The other three methods mentioned in Sec. III are also used to validate our arguments. The three methods [27–29] and the present method are denoted by M_1 , M_2 , M_3 , and M_p , respectively. In the simulation, s_1 is set to be s_2 in M_2 , but to be 1.0 in other methods.

A. Steady Poiseuille flow

The first problem considered is a steady Poiseuille flow driven by a constant body force \mathbf{F} . The flow direction is set to be the positive direction of the x axial, thus $\mathbf{F} = [F_x, 0]$. The analytical solution for a channel of width $2L$ is

$$\mathbf{u}_a = \left[\frac{F_x}{2\nu}(L^2 - y^2), 0 \right]. \quad (26)$$

The periodic boundary conditions are used in the flow direction, while the standard half-way bounce-back boundary scheme is used for nonslip boundary conditions at the walls. Due to the simple flow configuration, the length of the channel is set to be $3\Delta x$ to save the computational load.

As analyzed by previous researchers [26,32], when the relaxation rate for the energy flux is chosen to be $s_3 = (16 - 8s_2)/(8 - s_2)$, no numerical slip occurs in the Poiseuille flow for the MRT LBM. To check its applicability in the CLBM with the present forcing scheme, we first choose kinematic viscosity $\nu = 0.5$, $F_x = 0.01$, and only three nodes are used to cover the channel width ($2L = 3\Delta x$). We change s_3 from 0.2 to 1.8 with a 0.05 interval, and the other parameters are set equal to s_2 . The residual error $E_R < 1 \times 10^{-9}$ is used as the convergence criterion, and the relative error E_2 is calculated for the following analysis:

$$E_R = \sqrt{\frac{\sum (\mathbf{u}_{(t+1000\delta t)} - \mathbf{u}_t)^2}{\sum \mathbf{u}_{(t+1000\delta t)}^2}}, \quad E_2 = \sqrt{\frac{\sum (\mathbf{u} - \mathbf{u}_a)^2}{\sum \mathbf{u}_a^2}}, \quad (27)$$

where the summation operator \sum is over all grid nodes. For this case, the needed value of s_3 for the nonslip rule is 1.6. As shown in Fig. 1, the relative error for each method changes with different values of s_3 . But only in the present method, the minimum value of E_2 is achieved when $s_3 = 1.6$. And when the nonslip condition is satisfied, the relative error reaches an extremely small value even in a very coarse mesh.

To further confirm the consistent nonslip boundary condition in the present method, we conduct several other cases. Now the channel width is set to be $50\Delta x$, and different body forces $F_x = [1 \times 10^{-6}, 3 \times 10^{-6}, 5 \times 10^{-6}, 7 \times 10^{-6}]$ are considered. The configurations are the same as those in Ref. [27], s_3 is chosen according to the nonslip rule, while other relaxation

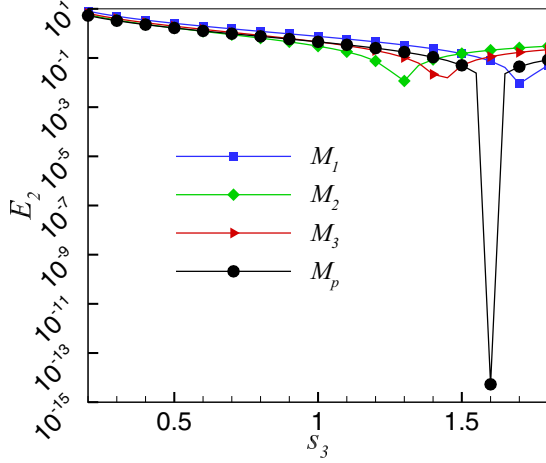


FIG. 1. Comparison of relative errors of different forcing schemes E_2 , as defined in Eq. (27), as a function of s_3 , in steady Poiseuille flow.

parameters are 1.754. As shown in Table I, the relative errors for M_1 are $O(10^{-4})$, which are consistent with the results in Ref. [27]. The small differences among the relative errors here and in Ref. [27] are related to the different choices for s_3 (the nonslip rule was not considered in Ref. [27]). Compared with these three methods, the relative errors for the present method are 5–6 orders of magnitude smaller, which confirms the conformation of the nonslip rule in the present method. From the discussion in Sec. III D, it is easy to observe that the error terms in the three methods M_1 , M_2 , and M_3 are in a descending order.

B. Steady Taylor-Green flow

For the two-dimensional steady incompressible flow in a periodic box $N \times N$, if the force field is given by

$$\mathbf{F}(x, y) = 2\nu u_0 \phi^2 [\cos(\phi x) \cos(\phi y), \sin(\phi x) \sin(\phi y)], \quad (28)$$

the flow has the following analytical solution:

$$\begin{aligned} \mathbf{u}_a(x, y) &= u_0 [\sin(\phi x) \sin(\phi y), \cos(\phi x) \cos(\phi y)], p_a(x, y) \\ &= p_0 + 0.25u_0^2 [\cos(2\phi x) - \cos(2\phi y)], \end{aligned} \quad (29)$$

where $\phi = 2\pi/N$, $p_0 = \rho_0 c_s^2$, and $\rho_0 = 1$. The flow is known as steady Taylor-Green flow or four-rolls mill [38], and is characterized by the Reynolds number, $Re = u_0 \pi / \nu$. In the simulation, the computational domain is covered by a series of grid nodes, $N/\Delta x = [10, 20, 40, 80]$, with three different conditions of $Re = [50, 100, 150]$. To weaken the artificial compressibility, $u_0 = 0.05$ is used in all the cases, s_b is given

TABLE I. Relative errors ($\times 10^4$) of different forcing schemes in steady Poiseuille flow. A series of body forces are considered, and s_3 is chosen according to the nonslip rule.

F_x	M_1	M_2	M_3	M_p
1×10^{-6}	2.739	2.339	1.113	1.044×10^{-6}
3×10^{-6}	2.739	2.339	1.113	3.173×10^{-6}
5×10^{-6}	2.739	2.339	1.113	5.527×10^{-6}
7×10^{-6}	2.739	2.339	1.113	7.296×10^{-6}

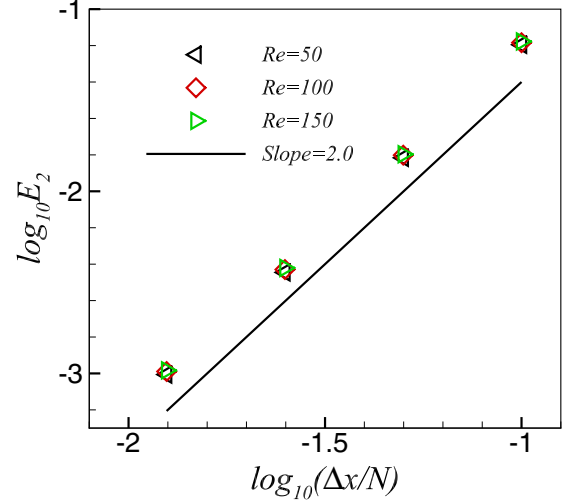


FIG. 2. The second-order accuracy of the new consistent forcing scheme, as measured by the relative errors E_2 , defined in Eq. (27), as a function of grid sizes in steady Taylor-Green flow at $Re = 50, 100$, and 150 .

equal to s_2 , while the remaining relaxation parameters are set to unity. The relative error E_2 is computed from Eq. (27).

The relationship between grid sizes and measured relative errors, E_2 , for the present forcing scheme at different Reynolds numbers is presented in Fig. 2. The slopes at $Re = 50, 100$, and 150 are 2.0133, 2.0076, and 2.0068, respectively. This demonstrates that the scheme proposed has second-order accuracy in space. The relative errors for different methods are shown in Table II. It is found that the present scheme achieves the smallest relative error for every grid resolution at every Reynolds number. Due to the discrete equilibrium central moments used in M_3 (see Eq. (10) in Ref. [39]), some additional errors are introduced into the CLBM, and this effect becomes evident when the mesh size is small. It may be the reason why this method manifests an outlier for the finest grid resolution. Generally, each method presents a second-order convergence rate.

C. Single static droplet

To validate the present forcing scheme for a complex force field, we consider the simulations of a static droplet using the Shan-Chen multiphase model [4], which is also known as the pseudopotential approach in the multiphase flow. The interaction force is calculated from an interaction potential $\psi(\mathbf{x})$ [4],

$$\mathbf{F} = -G\psi(\mathbf{x}) \sum_i w_i \psi(\mathbf{x} + \mathbf{e}_i \Delta t) \mathbf{e}_i, \quad (30)$$

where G is used to control the interaction strength and w_i are the weights. When only the nearest-neighbor interactions are considered on the D2Q9 lattice, $w_i = 1/3$ for $|\mathbf{e}_i|^2 = 1$ and $w_i = 1/12$ for $|\mathbf{e}_i|^2 = 2$. The exponential form of the pseudopotential is used, i.e., $\psi(\rho) = \psi_0 \exp(-\rho_0/\rho)$. Let us denote ρ_V and ρ_L as the vapor and liquid coexistence densities, respectively. In this study, $\psi_0 = 1$, $\rho_0 = 1$, and $G = 10/3$ are used, which leads to $\rho_V = 0.3675$ and $\rho_L = 2.783$ [40,41]. The simulations are conducted in a periodic box $N \times N =$

TABLE II. Relative errors ($\times 10^2$) and convergence rates (CR) achieved by different forcing schemes at different Reynolds numbers in steady Taylor-Green flow.

$N/\Delta x$	Re = 50				Re = 100				Re = 150			
	M_P	M_1	M_2	M_3	M_P	M_1	M_2	M_3	M_P	M_1	M_2	M_3
10	6.3752	6.5748	6.5522	6.3959	6.5448	6.6456	6.6398	6.5660	6.6482	6.7162	6.7135	6.6698
20	1.5275	1.6263	1.6051	1.5538	1.5788	1.6283	1.6227	1.6063	1.5974	1.6305	1.6279	1.6261
40	0.3587	0.3969	0.3782	0.3843	0.3719	0.3961	0.3909	0.4074	0.3796	0.3957	0.3933	0.4145
80	0.0986	0.1141	0.1037	0.1498	0.1025	0.1109	0.1076	0.1543	0.1040	0.1098	0.1082	0.1560
CR	2.0133	1.9579	2.0031	1.8264	2.0076	1.9753	1.9896	1.8213	2.0068	1.9848	1.9917	1.8222

250×250 . A round droplet of radius $R = 50$ is initialized by setting $\rho = \rho_L$ in the circle and $\rho = \rho_V$ outside the circle. The relaxation parameters are chosen as $s_b = s_2 = 1.4$.

The steady-state density contours for varied s_3 obtained by different forcing schemes are compared in Fig. 3. The

inserted dashed circle represents the theoretical location of the droplet. From the first column of Fig. 3 (obtained by the forcing scheme of Premnath *et al.* [27]), it can be seen that the shape of the droplet is s_3 -dependent and it changes from a noncircular shape to a round one with the increase

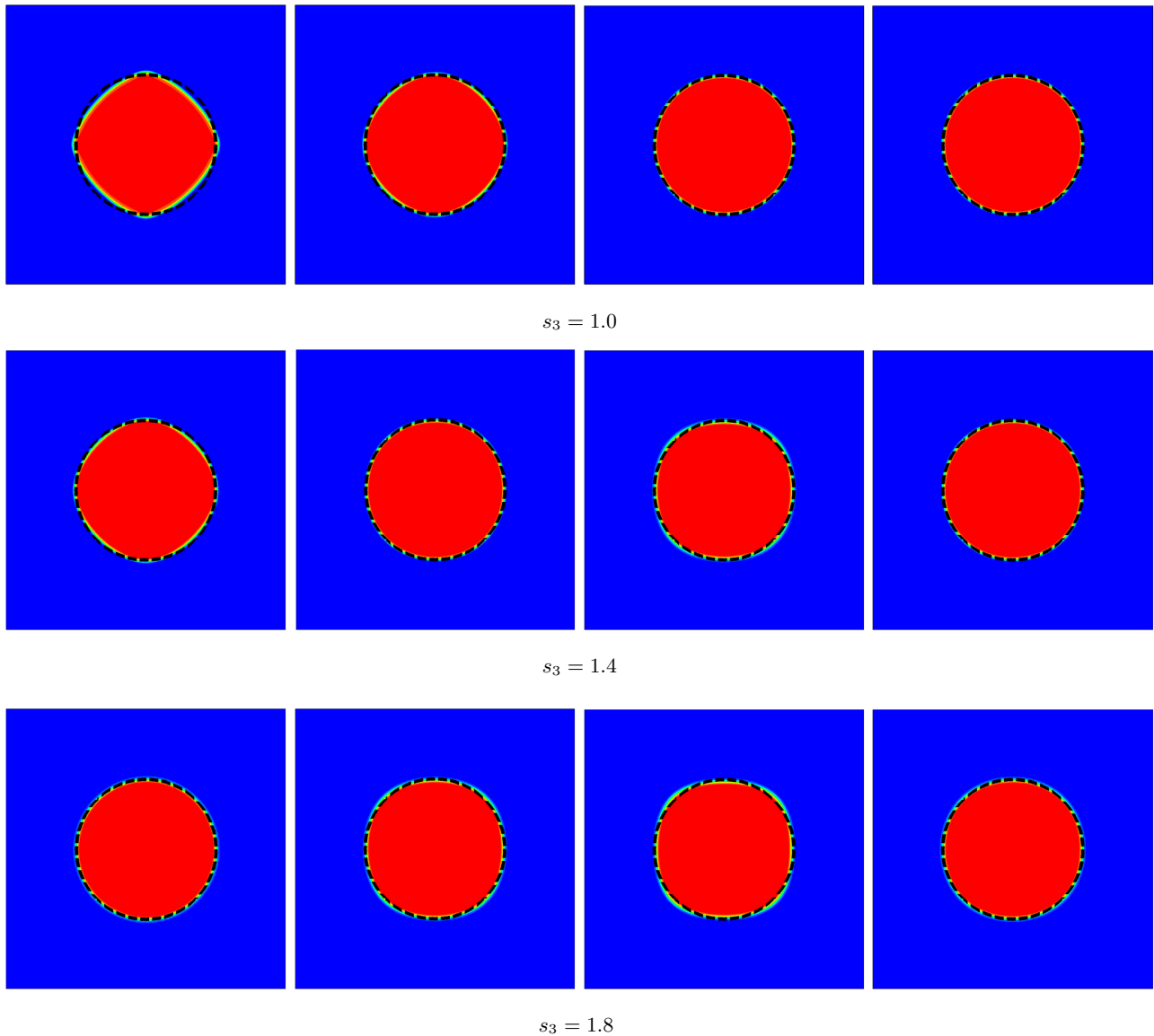


FIG. 3. Steady-state density contours of single static droplet for varied s_3 , achieved by different forcing schemes (from left to right): Premnath *et al.* [27] (first column), Lycett-Brown and Luo [28] (second column), De Rosi [29] (third column) and the new forcing scheme (fourth column). The additional dashed circle is the theoretical location of the droplet.

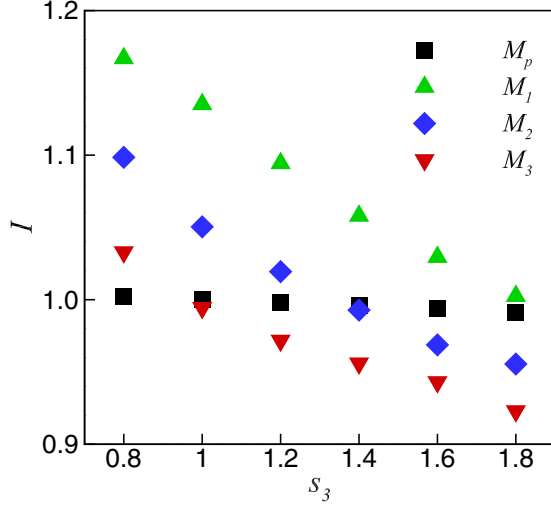


FIG. 4. Isotropy defined by $I = |R_{\pi/4}/R_0|$, as a function of s_3 for different forcing schemes for single static droplet simulation.

of s_3 . As discussed in Sec. III A, the removal of high-order terms for the central moments of Δf in Ref. [27] introduces inconsistencies with the scheme proposed by Guo *et al.* [25]. Only when s_3 is set to be 2.0, the inconsistency can be eliminated. Although we cannot give the result with $s_3 = 2.0$ (divergent for this simulation), the tendency confirms our argument. Analogously, as discussed in Secs. III B and III C, the inconsistencies in M_2 and M_3 can only be eliminated under the conditions of $s_3 = s_2$ and $s_3 = 1.0$, respectively, which is also confirmed in the figure. For the present forcing scheme, the droplet is always in round shape independent of the value of s_3 , as can be seen in the last column of Fig. 3.

To quantify the inconsistency, we define an isotropy parameter as $I = |R_{\pi/4}/R_0|$, where the subscript denotes the angle between the x axis and the line along which the radius is measured. From Fig. 4, we can see two clear trends: I in the present forcing scheme is almost independent of s_3 (the maximal relative variation is less than 1%), while I depends on s_3 apparently in the other methods and the anisotropies can only be eliminated under certain conditions as discussed in Sec. III D.

APPENDIX

The raw moments can be transformed to the discrete DFs through \mathbf{M}^{-1} , and the central moments can be shifted to raw moments through \mathbf{N}^{-1} ,

$$|f_i\rangle = \mathbf{M}^{-1}|T_i\rangle, \quad |T_i\rangle = \mathbf{N}^{-1}|\tilde{T}_i\rangle. \quad (\text{A1})$$

The explicit expressions for \mathbf{M}^{-1} and \mathbf{N}^{-1} are

$$\mathbf{M}^{-1} = \begin{bmatrix} 1 & 0 & 0 & -1 & 0 & 0 & 0 & 0 & 1 \\ 0 & 1/2 & 0 & 1/4 & 1/4 & 0 & 0 & -1/2 & -1/2 \\ 0 & 0 & 1/2 & 1/4 & -1/4 & 0 & -1/2 & 0 & -1/2 \\ 0 & -1/2 & 0 & 1/4 & 1/4 & 0 & 0 & 1/2 & -1/2 \\ 0 & 0 & -1/2 & 1/4 & -1/4 & 0 & 1/2 & 0 & -1/2 \\ 0 & 0 & 0 & 0 & 0 & 1/4 & 1/4 & 1/4 & 1/4 \\ 0 & 0 & 0 & 0 & 0 & -1/4 & 1/4 & -1/4 & 1/4 \\ 0 & 0 & 0 & 0 & 0 & 1/4 & -1/4 & -1/4 & 1/4 \\ 0 & 0 & 0 & 0 & 0 & -1/4 & -1/4 & 1/4 & 1/4 \end{bmatrix}, \quad (\text{A2})$$

V. CONCLUSIONS

In this study, we present an alternative derivation of the cascaded lattice Boltzmann method. A shift matrix \mathbf{N} is introduced in the derivation, by which the raw moments of the discrete distribution function are shifted to their central moments. This approach puts the MRT LBM and CLBM into a unified general framework and clarifies the relationship between them. Based on this, a new method to incorporate forcing terms into the CLBM is proposed.

The forcing terms are incorporated by means of central moments, which is compatible with the basic ideology of CLBM. According to the definition of the shift matrix \mathbf{N} , CLBM degrades into an MRT LBM when \mathbf{N} is a unit matrix. The present forcing scheme retains the property of and degrades into the Guo forcing scheme in the MRT LBM when \mathbf{N} is a unit matrix. Specifically, the present forcing scheme degrades to the original forcing scheme proposed by Guo *et al.* when all the relaxation parameters are set to be the same. Numerical simulations for several benchmark problems confirm the consistency of the nonslip rule, the second-order accuracy in space, and the property of isotropy for the present forcing scheme. In the meantime, some inconsistencies in the previous forcing schemes are also revealed.

The derivation and the method developed are quite intelligible, and no cumbersome operations are involved in the practical implementation. For other discrete velocity models (for example, D3Q15, D3Q19, and D3Q27), the corresponding methods can be developed directly by finding corresponding raw moments sets and obtaining the expressions of \mathbf{M} , \mathbf{N} , and C_i . Further work will demonstrate that the present method can be extended to three dimensions (3D) readily.

ACKNOWLEDGMENTS

The authors thank Dr. Chuandong Lin for fruitful discussions. Support from the MOST National Key Research and Development Programme (Project No. 2016YFB0600805) and the Center for Combustion Energy at Tsinghua University is gratefully acknowledged. Supercomputing time on ARCHER is provided by the UK Consortium on Mesoscale Engineering Sciences (UKCOMES) under the UK Engineering and Physical Sciences Research Council Grant No. EP/L00030X/1.

and

$$\mathbf{N}^{-1} = \begin{bmatrix} 1 & 0 & 0 & 0 & 0 & 0 & 0 & 0 & 0 \\ u_x & 1 & 0 & 0 & 0 & 0 & 0 & 0 & 0 \\ u_y & 0 & 1 & 0 & 0 & 0 & 0 & 0 & 0 \\ u_x^2 + u_y^2 & 2u_x & 2u_y & 1 & 0 & 0 & 0 & 0 & 0 \\ u_x^2 - u_y^2 & 2u_x & -2u_y & 0 & 1 & 0 & 0 & 0 & 0 \\ u_x u_y & u_y & u_x & 0 & 0 & 1 & 0 & 0 & 0 \\ u_x^2 u_y & 2u_x u_y & u_x^2 & u_y/2 & u_y/2 & 2u_x & 1 & 0 & 0 \\ u_y^2 u_x & u_y^2 & 2u_x u_y & u_x/2 & -u_x/2 & 2u_y & 0 & 1 & 0 \\ u_x^2 u_y^2 & 2u_x u_y^2 & 2u_y u_x^2 & u_x^2/2 + u_y^2/2 & u_y^2/2 - u_x^2/2 & 4u_x u_y & 2u_y & 2u_x & 1 \end{bmatrix}. \quad (\text{A3})$$

[1] Y.-H. Qian, S. Succi, and S. A. Orszag, *Annu. Rev. Comput. Phys.* **3**, 195 (1995).

[2] S. Chen and G. D. Doolen, *Annu. Rev. Fluid Mech.* **30**, 329 (1998).

[3] S. Succi, *The Lattice Boltzmann Equation: For Fluid Dynamics and Beyond* (Oxford University Press, Oxford, 2001).

[4] X. Shan and H. Chen, *Phys. Rev. E* **47**, 1815 (1993).

[5] Z. Guo and C. Shu, *Lattice Boltzmann Method and Its Applications in Engineering*, Vol. 3 (World Scientific, Singapore, 2013).

[6] W. Gong, Y. Zu, S. Chen, and Y. Yan, *Sci. Bull.* **62**, 136 (2016).

[7] C. Lin, A. Xu, G. Zhang, and Y. Li, *Combust. Flame* **164**, 137 (2016).

[8] C. Lin, A. Xu, G. Zhang, Y. Li, and S. Succi, *Phys. Rev. E* **89**, 013307 (2014).

[9] Q. Li, K. H. Luo, Q. Kang, Y. He, Q. Chen, and Q. Liu, *Prog. Energy Combust. Sci.* **52**, 62 (2016).

[10] Y. Qian, D. d’Humières, and P. Lallemand, *Europhys. Lett.* **17**, 479 (1992).

[11] D. d’Humières, *Prog. Astronaut. Aeronaut.* **159**, 450 (1994).

[12] M. Geier, A. Greiner, and J. G. Korvink, *Phys. Rev. E* **73**, 066705 (2006).

[13] P. Lallemand and L.-S. Luo, *Phys. Rev. E* **61**, 6546 (2000).

[14] D. Lycett-Brown and K. H. Luo, *Phys. Rev. E* **94**, 053313 (2016).

[15] L. Fei and K. H. Luo, *arXiv:1610.07114* (2016).

[16] I. Ginzburg, *Adv. Water Res.* **28**, 1171 (2005).

[17] I. Ginzburg, F. Verhaeghe, and D. d’Humières, *Commun. Comput. Phys.* **3**, 427 (2008).

[18] S. Ansumali, I. V. Karlin, and H. C. Öttinger, *Europhys. Lett.* **63**, 798 (2003).

[19] S. Ansumali and I. V. Karlin, *Phys. Rev. E* **62**, 7999 (2000).

[20] X. He, S. Chen, and R. Zhang, *J. Comput. Phys.* **152**, 642 (1999).

[21] J. M. Buick and C. A. Greated, *Phys. Rev. E* **61**, 5307 (2000).

[22] A. Ladd and R. Verberg, *J. Stat. Phys.* **104**, 1191 (2001).

[23] X. He, X. Shan, and G. D. Doolen, *Phys. Rev. E* **57**, R13 (1998).

[24] X. He, S. Chen, and G. D. Doolen, *J. Comput. Phys.* **146**, 282 (1998).

[25] Z. Guo, C. Zheng, and B. Shi, *Phys. Rev. E* **65**, 046308 (2002).

[26] Z. Guo and C. Zheng, *Int. J. Comput. Fluid Dynam.* **22**, 465 (2008).

[27] K. N. Premnath and S. Banerjee, *Phys. Rev. E* **80**, 036702 (2009).

[28] D. Lycett-Brown and K. H. Luo, *Comput. Math. Appl.* **67**, 350 (2014).

[29] A. De Rosis, *Phys. Rev. E* **95**, 023311 (2017).

[30] P. Asinari, *Phys. Rev. E* **78**, 016701 (2008).

[31] Q. Liu, Y.-L. He, D. Li, and Q. Li, *Int. J. Heat Mass Transfer* **102**, 1334 (2016).

[32] I. Ginzburg and D. d’Humières, *Phys. Rev. E* **68**, 066614 (2003).

[33] A. Kupershtokh, D. Medvedev, and D. Karpov, *Comput. Math. Appl.* **58**, 965 (2009).

[34] H. Huang, M. Krafczyk, and X. Lu, *Phys. Rev. E* **84**, 046710 (2011).

[35] Q. Li, K. H. Luo, and X. J. Li, *Phys. Rev. E* **86**, 016709 (2012).

[36] D. Lycett-Brown and K. H. Luo, *Phys. Rev. E* **91**, 023305 (2015).

[37] R. K. Freitas, A. Henze, M. Meinke, and W. Schröder, *Comput. Fluids* **47**, 115 (2011).

[38] G. Taylor, *Proc. R. Soc. London A* **146**, 501 (1934).

[39] A. De Rosis, *Europhys. Lett.* **116**, 44003 (2017).

[40] Z. Yu and L.-S. Fan, *J. Comput. Phys.* **228**, 6456 (2009).

[41] Q. Li, P. Zhou, and H. J. Yan, *Phys. Rev. E* **94**, 043313 (2016).